

Sliding-Mode PID Control of UAV Based on Particle Swarm Parameter Tuning

Yunping Liu^{1,2,*}, Xingxing Yan¹, Fei Yan¹, Ze Xu¹ and Weiyan Shang³

Abstract: Due to the coupled motion between the rotor unmanned aerial vehicle (UAV) and the manipulator, the underactuation characteristics of the system itself, and the influence of external uncertainties, the stability of the rotor UAV's manipulator control system is difficult to control. Based on the dynamic model of the rotor UAV, the stability of the whole UAV manipulator control system is improved by using the piecewise cost function, the compression factor particle swarm optimization (PSO) algorithm and the sliding mode PID to establish the sliding mode PID control stability method based on the PSO. Compared with the sliding mode PID control method, this method solves the serious buffeting problem in the sliding mode control, reduces the influence of the external disturbance and realizes the attitude stabilization control of the UAV manipulator quickly and accurately, thus shortens the system adjustment time and improves the anti-interference ability.

Keywords: Manipulator, dynamic model, compression factor, particle swarm, sliding mode PID, UAV.

1 Introduction

The intrinsic characteristics of coupled motion, underactuation, multivariable and non-linearity between the rotor UAV and the manipulator make it easy to produce problems such as jitter and instability under the effects of external gyro effects and atmospheric disturbances. The cost of the UAV carrying equipment is higher and the probability of accident is larger. Therefore, the stability control of the rotor flight manipulator has attracted more and more attention and research by experts and scholars at home and abroad [Liu, Li, Wang et al. (2016); Xiang, Liu, Su et al. (2017)].

At present, many typical algorithms have been developed for UAV flight control, including PID control algorithm, sliding mode control, adaptive algorithm, Backstepping, self-adaption, state feedback method [Ran, Wang, Hou et al. (2014)] and other nonlinear control methods. Sliding mode control has the advantages of fast response, insensitivity

¹ School of Automation, Nanjing University of Information Science and Technology, Collaborative Innovation Center of Atmospheric Environment and Equipment, Nanjing, 210044, China.

² Department of Mechanical and Industrial Engineering, Ryerson University, Toronto, M5B 2K3, Canada.

³ Department of Mechanical and Manufacturing Engineering, University of Manitoba, Winnipeg, R3T 5V6, Canada.

* Corresponding Author: Yunping Liu. Email: liuyunping@nuist.edu.cn.

Received: 10 January 2019; Accepted: 23 January 2019.

to parameter changes and disturbances, no need for system on-line edge, physical realization, etc., but it also has chattering, a non-negligible disadvantage, and therefore needs to be improved and applied to control of quadrotor. Literature Merheb et al. [Merheb, Noura and Bateman (2014)] proposed an active fault-tolerant controller with sliding mode observer and sliding mode control for fault-tolerant control of quadrotor UAVs. Literature Zheng et al. [Zheng, Xiong and Luo (2014)] proposed a method based on two-order sliding mode control (2-SMC) to control quadrotor UAV. Literature Chen et al. [Chen, Jiang, Zhang et al. (2016)] proposed a robust nonlinear controller combined with sliding mode control technology and background control technology. Literature Wang et al. [Wang, Ju, Gao et al. (2018)] proposed a coverage control algorithm based on particle swarm optimization algorithm, which can improve the efficiency of cluster coverage.

At present, there are few studies on rotor UAVs equipped with manipulators at home and abroad. Literature Mebarki et al. [Mebarki and Lippiello (2014)] reviewed the main research achievements of the flight robot system and corresponding dynamic modeling and coupling analysis, autonomous control and other aspects, and analyzed and forecasted the key problems and difficulties. In the literature Karagulle et al. [Karagulle, Malgaca, Dirilmis et al. (2015)], the frequency characteristics of the flexible manipulator were studied through Matlab simulation, and the controllability of the vibration signal was analyzed. In literature Xie et al. [Xie, Zhao and Cai (2013)], flexible manipulator dynamics modeling and dynamics control and other related problems, the rotational algebra method, the method based on Lagrange equation and the model identification method in the dynamic modeling of flexible manipulator were introduced. In literature Purwar et al. [Purwar, Kar and Jha (2004)], based on the analysis of the interaction dynamics of each other, the overall dynamics model was established, and a predictive controller was designed to eliminate the position and attitude error of the terminal actuator. Literature Tran et al. [Tran and Kang (2016)] presented an augmented adaptive control scheme for tracking the inertial space desired trajectory of the end manipulator of space manipulator when the system parameters are unknown. In the above three literature, although the manipulator can be controlled more accurately and efficiently, the stability of the entire system is lacking.

In this paper, based on the traditional sliding mode control algorithm, a segmented cost function, a compression factor particle swarm parameter tuning algorithm and a sliding mode PID algorithm are added, so that in the design of UAV controller, it also has the advantages of compression factor particle swarm parameter tuning algorithm of segmented cost function and sliding mode PID control, the system can not only achieve stable control of the manipulator, but also maintain the stability of the system while the manipulator moves, and improve the response speed and robustness of the entire system.

2 System dynamic modeling

Taking the structural diagram of the rotor-flying manipulator shown in Fig. 1 as an example, its coordinate system is established: Earth coordinate system E-XYZ, four-rotor coordinate system B-xyz and robot arm coordinate system A-ax, az. Among them, B is the location of the center of mass of the origin at the quadrotor. Tab. 1 is a description of some of the symbols in the paper.

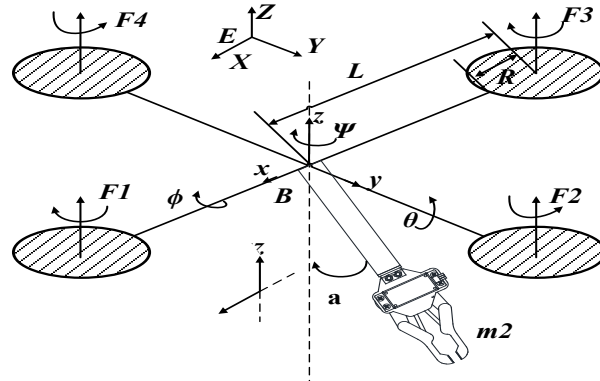


Figure 1: Figure of arm structure of UAV

Table 1: Symbol description

Number	Symbol	Symbol description
1	m_1	Quality of quadrotor UAV
2	m_2	Quality of the carrier
3	g	Local gravitational acceleration
4	L	Rotor center of mass to motor distance
5	C_T	Rotor lift coefficient
6	C_Q	Rotor torque coefficient
7	R	Rotor radius
8	ρ	Air density
9	I_x	Moment of inertia about the X-axis
10	I_y	Moment of inertia about the Y-axis
11	I_z	Moment of inertia about the Z-axis

The generalized coordinate vector $q = (\phi, \theta, \psi, x, y, z, a)^T$ and pseudo velocity vector $p = (p, q, r, u, v, w, b)^T$, based on the Euler-poincare equation, are used to establish the dynamic model [Duc, Trong and Xuan (2015)] of the quadrotor UAV. The general form of the equation is shown in Formulas 1 and 2.

$$\dot{q} = V(q)p \quad (1)$$

$$M(q)\dot{p} + C(q, p)p + F(p, q, u) = 0 \quad (2)$$

where, $\eta = (\phi, \theta, \psi)^T$ represents the attitude angular vector of the quadrotor aircraft, and $X = (x, y, z)^T$ represents the space position vector of the quadrotor aircraft centroid relative to the geodetic coordinate system. a represents the angle between the manipulator and the z axis, while b represents the angular velocity. $V(q)$ is the kinematics matrix, which is the matrix of the pseudo rotor speed to the generalized velocity of the quadrotor. $M(q)$ is the inertia matrix, $C(q, p)$ is the gyroscopic matrix, and $F(p, q, u)$ is the sum of aerodynamic force, gravity and control input. To simplify the formula, let $S_\phi = \sin\phi, S_\theta = \sin\theta, S_a = \sin a, C_\theta = \cos\theta, S_\psi = \sin\psi, C_\psi = \cos\psi, C_a = \cos a$.

The expressions in the above are as follows:

$$F(p, q, u) = \begin{bmatrix} -LU_2 + gm_2RC_aC_\theta S_f \\ -LU_3 + gm_2R(C_\theta C_f S_a + C_a S_\theta) \\ -LU_4 - gm_2RC_\theta S_a S_f \\ -g(m_1 + m_2)S_\theta \\ g(m_1 + m_2)C_\theta S_f \\ -U_1 + g(m_1 + m_2)C_\theta C_f \\ -T + gm_2R(C_\theta C_f S_a + C_a S_\theta) \end{bmatrix} \quad (3)$$

In the above formula, $M = [b_1, b_2]$ and $C(q, p) = [a_1 \ a_2 \ a_3 \ a_4 \ a_5 \ a_6 \ a_7]$.

Among them, $b_1, b_2, a_1, a_2, a_3, a_4, a_5, a_6, a_7$ are submatrices, which are defined as follows:

$$b_1 = \begin{bmatrix} I_x + m_2 R^2 C_a^2 & 0 & -m_2 R^2 C_a S_a \\ 0 & I_y + J_y + m_2 R^2 & 0 \\ -m_2 R^2 C_a S_a & 0 & I_z + m_2 R^2 S_a^2 \\ 0 & -m_2 R C_a & 0 \\ m_2 R C_a & 0 & -m_2 R S_a \\ 0 & m_2 R S_a & 0 \\ 0 & J_y + m_2 R^2 & 0 \end{bmatrix} \quad (4)$$

$$b_2 = \begin{bmatrix} 0 & m_2 R C_a & 0 & 0 \\ -m_2 R C_a & 0 & m_2 R S_a & J_y + m_2 R^2 \\ 0 & m_2 R S_a & 0 & 0 \\ m_1 + m_2 & 0 & 0 & -m_2 R C_a \\ 0 & m_1 + m_2 & 0 & 0 \\ 0 & 0 & m_1 + m_2 & m_2 R S_a \\ -m_2 R C_a & 0 & m_2 R S_a & J_y + m_2 R^2 \end{bmatrix} \quad (5)$$

$$a_1 = \begin{bmatrix} -m_2 R C_a (w + q R S_a) \\ I_x r + m_2 R^2 C_a (r C_a + p S_a) \\ -I_x q + m_2 R C_a (u - q R C_a) \\ -m_2 r R C_a \\ 0 \\ m_2 p R C_a \\ \frac{1}{2} m_2 R (r R C_a + (v + 2 p R C_a) S_a) \end{bmatrix} \quad (6)$$

$$a_2 = \begin{bmatrix} -r(I_y + J_y + m_2 R^2) + m_2 R v S_a \\ -m_2 R(w C_a + u S_a) \\ p(I_y + J_y + m_2 R^2) + m_2 R v C_a \\ m_2 q R S_a \\ -m_2 R(r C_a + p S_a) \\ m_2 q R C_a \\ -\frac{I}{2} m_2 R(w C_a + u S_a) \end{bmatrix} \quad (7)$$

$$a_3 = \begin{bmatrix} -r(I_y + J_y + m_2 R^2) + m_2 R v S_a \\ -I_z p - m_2 R^2 S_a (r C_a + p S_a) \\ m_2 R(-u + q R C_a) S_a \\ m_2 r R S_a \\ 0 \\ -m_2 p R S_a \end{bmatrix} \quad (8)$$

$$a_4 = \begin{bmatrix} m_2 r R C_a \\ (m_1 + m_2) w \\ -(m_1 + m_2) v - m_2 p R C_a \\ 0 \\ (m_1 + m_2) r \\ -(m_1 + m_2) q \\ -\frac{I}{2} m_2 (b + q) R S_a \end{bmatrix} \quad (9)$$

$$a_5 = \begin{bmatrix} -(m_1 + m_2) w - m_2 q R S_a \\ m_2 R(r C_a + p S_a) \\ (m_1 + m_2) u - m_2 q R C_a \\ -(m_1 + m_2) r \\ 0 \\ (m_1 + m_2) p \\ \frac{I}{2} m_2 R(r C_a + p S_a) \end{bmatrix} \quad (10)$$

$$a_6 = \begin{bmatrix} (m_1+m_2)v - m_2 r R S_a \\ -(m_1+m_2)u \\ m_2 p R S_a \\ (m_1+m_2)q \\ -(m_1+m_2)p \\ 0 \\ -\frac{1}{2}m_2(b+q)RC_a \end{bmatrix} \quad (11)$$

$$a_7 = \begin{bmatrix} -r(J_y + m_2 R^2) - m_2 R^2 (rC_{2a} + pS_{2a}) \\ 0 \\ p(J_y + m_2 R^2) + m_2 R^2 (-pC_{2a} + rS_{2a}) \\ m_2(b+2q)RS_a \\ -2m_2 R (rC_a + pS_a) \\ m_2(b+2q)RC_a \\ \frac{1}{2}m_2 R (wC_a + uS_a) \end{bmatrix} \quad (12)$$

U_1 =Vertical height controlled variable;
 U_2 =Roll input controlled variable;
 U_3 =Pitch control input;
 U_4 =Yaw control;
 T =Controlled variable of the dropdown angle;
 $F_i(i=1,2,3,4)$ =The pulling force of each rotor;
 $A = \pi R^2$, and

$$\begin{cases} U_1 = F_1 + F_2 + F_3 + F_4 \\ U_2 = F_2 - F_4 \\ U_3 = F_1 - F_3 \\ U_4 = F_1 - F_2 + F_3 - F_4 \\ F = \frac{1}{2}\rho AC_T R^2 \Omega^2 \end{cases} \quad (13)$$

Input vector is $U = [U_1, U_2, U_3, U_4, T]^T$. When the quadrotor is flying at low speed in a state where there is no wind or the wind speed is small, the air resistance has little

influence on the system and can be ignored. At the same time, it is assumed that the roll angle and pitch angle of the quadrotors during the flight are very small. And their rate of change is also sufficiently small, according to $V(q)$, it can be approximated as:

$$\begin{bmatrix} \dot{f} \\ \dot{\theta} \\ \dot{\psi} \end{bmatrix} = \begin{bmatrix} 1 & 0 & 0 \\ 0 & 1 & 0 \\ 0 & 0 & 1 \end{bmatrix} \begin{bmatrix} p \\ q \\ r \end{bmatrix} \quad (14)$$

Therefore, the mathematical model of the system can ultimately be simplified to:

$$\begin{cases} \ddot{f} = [L(2I_z(m_1+m_2) + m_1m_2R^2)(-LU_2C_{2a} + LU_4S_{2a})]/F \\ \ddot{\theta} = (-T + LU_3)/I_y \\ \ddot{\psi} = [L(2I_x(m_1+m_2) + m_1m_2R^2)U_4 + m_1m_2R^2(LU_4C_{2a} + U_2S_{2a})]/F \\ \ddot{x} = [-2m_2R(2b^2J_y(m_1+m_2) + 2b^2m_1m_2R^2 + 2m_2RU_1C_a)S_a]/A_4 \\ \quad + [4m_2(m_1+m_2)RTC_a + A_4*gS_\theta + g(I_x - I_z)m_1m_2R^2C_{2a}C_\theta S_f]/A_4 \\ \ddot{y} = [-g(2I_xI_z(m_1+m_2) + (I_x + I_z)m_1m_2R^2)C_\theta S_f]/F \\ \quad + (2I_xLm_2RU_4S_a - 2I_zLm_2RU_2C_a)/F \\ \ddot{z} = (A_1 + A_2*U_1 - A_3*T)/A_4 \\ \ddot{\alpha} = \{((I_y + J_y)(m_1+m_2) + m_1m_2R^2)T\}/[I_yJ_y(m_1+m_2) + I_y m_1m_2R^2] + \\ \quad - \{L(J_y(m_1+m_2) + m_1m_2R^2)U_3 - I_y m_2RU_1S_a\}/[I_yJ_y(m_1+m_2) + I_y m_1m_2R^2] \end{cases} \quad (15)$$

3 Controller design

The position control of quadrotor aircraft is divided into horizontal position control and height control. Considering the underactuation of the four rotors, that is, the 4 inputs control 6 degrees of freedom, we can make full use of the coupling characteristics of the system to establish the mathematical relationship between the attitude angle and the position and the height control, so that the trajectory tracking is realized by controlling the attitude angle and the height of the position. The system is divided into a full drive subsystem and an underactuated subsystem. Fig. 2 is a schematic diagram of control flow.

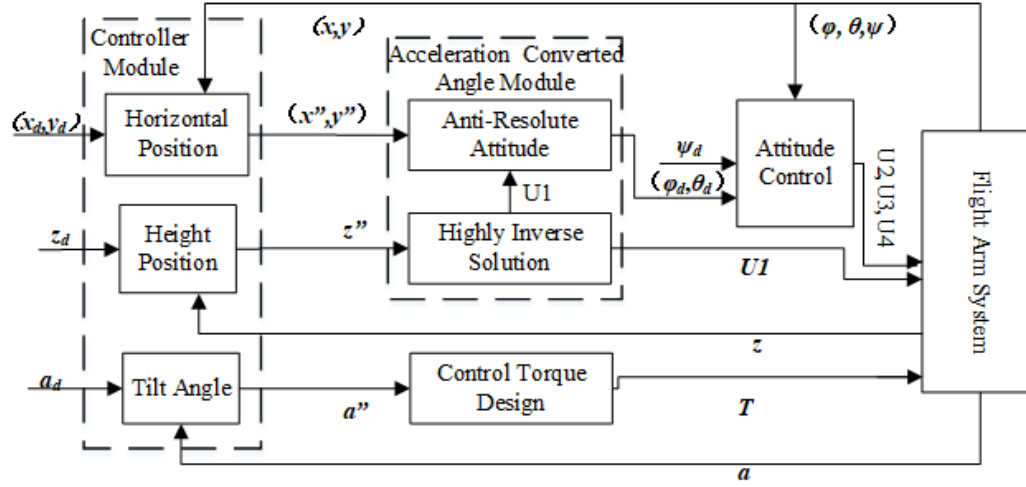


Figure 2: Figure of control flow diagram

Both the horizontal position control module and the drop down tilt module adopt PID algorithm. The relationship between the target position and acceleration, the desired inclination angle and the control torque of the manipulator is established. The control law of the three quantities is as follows:

$$\begin{aligned}
 \ddot{x} &= k_{p_1}(x_d - x) + k_{i_1} \int (x_d - x) dt + k_{d_1}(\dot{x}_d - \dot{x}) \\
 \ddot{y} &= k_{p_2}(y_d - y) + k_{i_2} \int (y_d - y) dt + k_{d_2}(\dot{y}_d - \dot{y}) \\
 T &= k_{p_3}(a_d - a) + k_{i_3} \int (a_d - a) dt + k_{d_3}(\dot{a}_d - \dot{a})
 \end{aligned} \tag{16}$$

The sliding mode PID algorithm is used for height control and attitude control. The design of sliding mode PID controller is mainly divided into two steps. One is to select the appropriate PID sliding mode surface function s and the other is to design an appropriate control law so that the system can reach and remain on the expected sliding surface $s = 0$. Taking the height control of the quadrotor as an example, firstly, it is known that z_d is the desired height and the actual height is z . The definition of the tracking error function is:

$$e_z = z_d - z \tag{17}$$

Select the sliding surface:

$$s_z = \dot{e}_z + d_1 * e_z + c_1 * \int e_z dt \tag{18}$$

where, \dot{s}_z is the derivative of s_z to time; both ε and k are positive constants. In the experiment, the value of ε is 0.01, the value of k is 3, and $sgn(s)$ is the sign function.

The Lyapunov function is used to judge the stability of the system and the positive definite function is set as follows:

$$\dot{s}_z = -\varepsilon \operatorname{sgn}(s_z) - ks_z \tag{19}$$

where, \dot{s}_z is the derivative of s_z to time; both ε and k are positive constants. In the experiment, the value of ε is 0.01, the value of k is 3, and $sgn(s)$ is the sign function.

The Lyapunov function is used to judge the stability of the system and the positive definite function is set as follows:

$$V_z = \frac{1}{2} s_z^2 > 0 \quad (20)$$

Its derivative along the trajectory is:

$$\dot{V}_z = s_z \dot{s}_z = s_z [-\varepsilon sgn(s_z) - k s_z] = -\varepsilon \|s_z\| - k \|s_z\|^2 < 0 \quad (21)$$

It can be seen that the quadrotor aircraft system meets the stability criterion of Lyapunov asymptotic stability and is an asymptotically stable system. That is, the tracking error will gradually decrease and eventually converge to zero, and the reachability condition of the sliding mode is satisfied. According to the first-order derivative of the sliding surface and the selected exponential reaching law, the concrete expression of the height of the entire system in the sliding mode can be obtained, as shown in Formula 22.

$$U_1 = (A_4 * s_z + A_3 * T - A_1) / A_2 \quad (22)$$

where,

$$\begin{aligned} A_1 &= -4g(m_1+m_2)(J_y(m_1+m_2)+m_1m_2R^2)C_\theta C_\varphi - m_2R(4\dot{a}^2 J_y(m_1+m_2)+4\dot{a}^2 m_1m_2R^2) * C_a \\ A_2 &= 2(2J_y(m_1+m_2)+m_2R^2(2m_1+m_2))-2m_2^2R^2C_{2a} \\ A_3 &= 4m_2(m_1+m_2)RS_a \\ A_4 &= 4(m_1+m_2)(J_y(m_1+m_2)+m_1m_2R^2) \end{aligned} \quad (23)$$

Similarly, the control laws for roll, pitch and yaw can be obtained as follows:

$$\begin{aligned} U_2 &= F((B * D - E * C) / (A * B - C^2)) \\ U_3 &= (I_y * G + T) / L \\ U_4 &= F((A * B * E - B * C * D) / (A * B * B - B * C^2)) \end{aligned} \quad (24)$$

Among them, D , G , E and T are the sliding surface functions of the roll, pitch, yaw and pull-down angles, A , b_l , C , F are respectively.

$$\begin{aligned} A &= L(2I_z(m_1+m_2)+m_1m_2R^2(1-C_{2a})) \\ B &= 2I_x(m_1+m_2)+m_1m_2R^2(1+C_{2a}) \\ C &= m_1m_2R^2S_{2a} \\ F &= 2(I_xI_z(m_1+m_2)+m_1m_2R^2(I_z \cos^2 a + I_xS_a^2)) \end{aligned} \quad (25)$$

4 Compression factor PSO algorithm for complex systems

The final convergence of system behavior can be controlled by using the constrain constraint factor, which can search different regions more effectively and obtain higher quality solutions. The specific operation is as follows: the speed updating formula of the

basic particle swarm algorithm is changed to:

$$\varphi = c_1 + c_2, \lambda = 2 / [2 - \varphi - \sqrt{(\varphi^2 - 4\varphi)}] J,$$

$$v_{id}(t+1) = \lambda \times v_{id}(t) + c_1 r_1(t)[p_{id}(t) - x_{id}(t)] + c_2 r_2(t)[p_{gd}(t) - x_{id}(t)].$$

Among them, λ is the compression factor. PSO algorithm with compression constraint factor [Sathya and Kayalvizhi (2014)] has faster convergence rate than standard PSO algorithm.

4.1 Compression factor PSO (PSO) optimization sliding mode PID

The compression factor PSO algorithm is used to optimize the flow chart of sliding mode PID [Faruk and Kikuchi (2011)], as shown in Fig. 3.

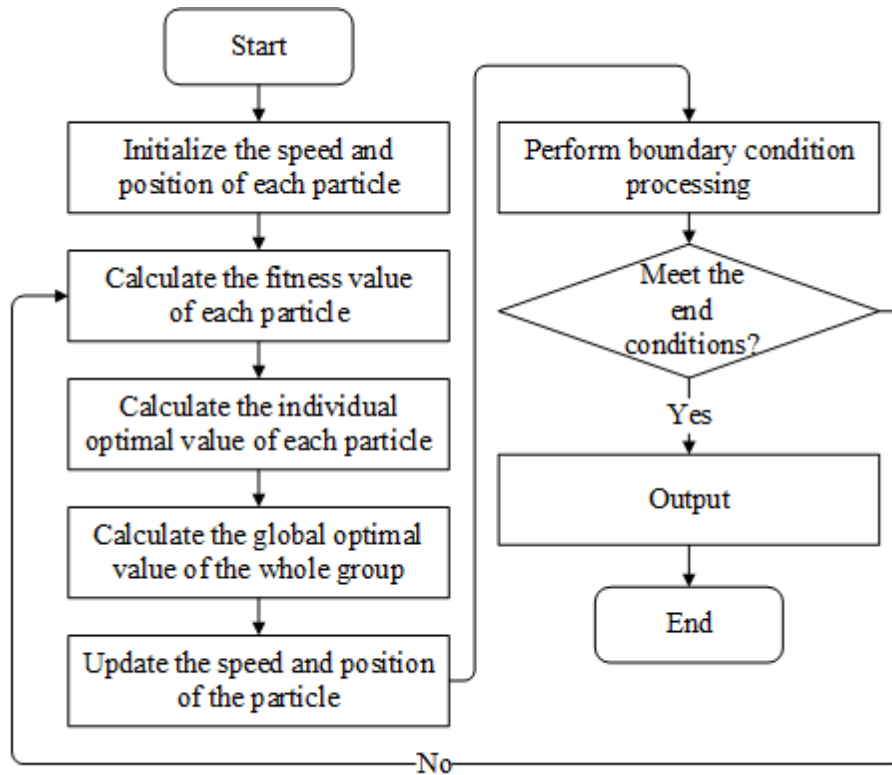


Figure 3: Compression factor PSO algorithm for sliding mode PID flow chart

4.2 Optimization of sliding mode PID parameters by compression factor PSO algorithm

The compression factor PSO algorithm is used to optimize the parameters of sliding mode PID k_p, k_i, k_d as follows:

- (1) The parameters are encoded with particles.
- (2) The population of particles is initialized, including population size N , position x_i and velocity v_i for each particle.

(3) The particle is decoded into a parameter value, and the cost function value J and the fitness function value f are obtained using this parameter, and $f=1/J$ is taken.

(4) For each particle, its fitness $f(i)$ is used to determine the extreme value $p_{best}(i)$ and the global extreme value g_{best} .

(5) The position x_i and speed v_i of the particle are iteratively updated.

Repeat steps (4) and (5) until the boundary conditions are satisfied and output results are obtained.

5 Compression factor PSO algorithm with piecewise cost function to optimize sliding mode PID algorithm

Assuming that the transfer function of the controlled object is $G(s)$, in order to obtain a satisfactory dynamic characteristic of the transition process, this paper uses the error absolute time integral performance index as the minimum objective function of the parameter selection. In order to prevent the control energy from being too large, the squared term of the control input is added to the objective function, and the following formula is used as the optimal index for parameter selection:

$$J_1 = \int_0^{\infty} (w_1 |e(t)| + w_2 u^2(t)) dt + w_3 t_u \quad (26)$$

where, $e(t)$ is error function; $u(t)$ is controller output; t_u is rise time, and w_1, w_2, w_3 are weights.

In order to avoid overshooting, the penalty function is used. That is, once overshoot occurs, the overshoot is regarded as the optimal index. The optimal indicator is:

$$J_2 = \int_0^{\infty} (w_1 |e(t)| + w_2 u^2(t) + w_4 |e(t)|) dt + w_3 t_u \quad (27)$$

where, $w_4 \gg w_1$.

That is, the final cost function is:

$$J = \begin{cases} \int_0^{\infty} (w_1 |e(t)| + w_2 u^2(t)) dt + w_3 t_u & e(t) \geq 0 \\ \int_0^{\infty} (w_1 |e(t)| + w_2 u^2(t) + w_4 |e(t)|) dt + w_3 t_u & e(t) < 0 \end{cases} \quad (28)$$

6 Simulation experiment and analysis

Based on the dynamic model of the rotor-flying manipulator established in Chapter 4, Simulink was used to simulate and analyze the model. Three modules were mainly built using S-Function, namely the controller module U , quadrotor power module Muav and fitness module. Simulation structure is shown in Fig. 4.

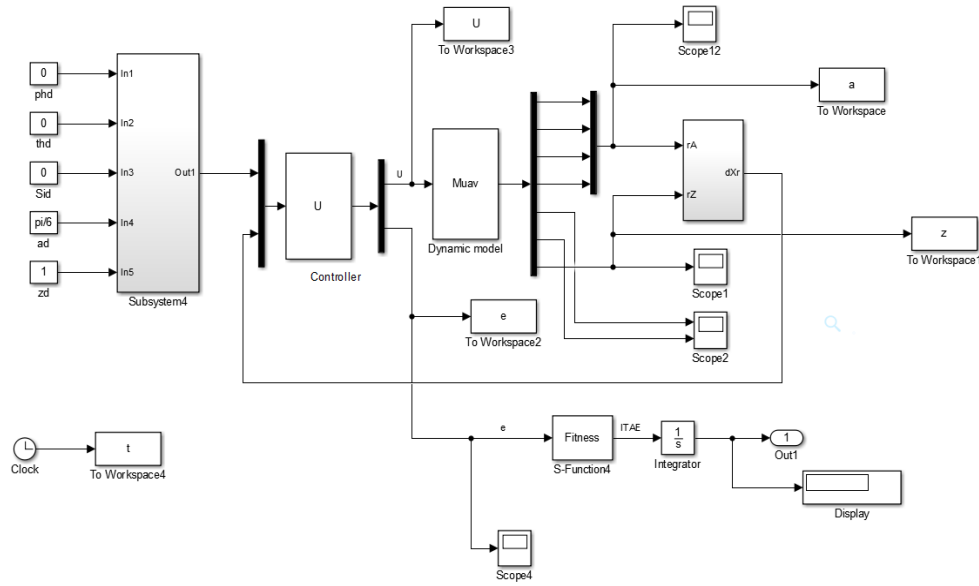


Figure 4: Simulink model of flight manipulator

For this model, the initial state is designed as:

$$x_0 = [\phi_0, \dot{\phi}_0, \theta_0, \dot{\theta}_0, \psi_0, \dot{\psi}_0, x_0, \dot{x}_0, y_0, \dot{y}_0, z_0, \dot{z}_0, a_0, b_0] \quad (29)$$

It is used to set the initial yaw angle of the quadrotor and the angle of the manipulator deviating from the center, as well as their angular velocity and speed. And the goal of expectation control is set as follows:

$$x \rightarrow x_d, y \rightarrow y_d, z \rightarrow z_d, \theta \rightarrow \theta_d, \psi \rightarrow \psi_d, f \rightarrow f_d, a \rightarrow a_d, b \rightarrow b_d \quad (30)$$

The initial state is set as: $x_0 = [0.1 \ 0 \ 0.05 \ 0 \ -0.1 \ 0 \ 0 \ 0 \ 0 \ 0 \ 1 \ 0 \ \pi/6 \ 0]^T$.

The expected values of each position are set as follows:

$$f_d=0, \theta_d=0, \phi_d=0, x_d=0, y_d=0, z_d=1, a_d=\pi/6.$$

Input the specific values of the hardware structure parameters of the quadrotor and manipulator of the Tab. 1 into the model, and set the relevant controller parameters. Tab. 2 is the specific setting of each parameter value entered into the model.

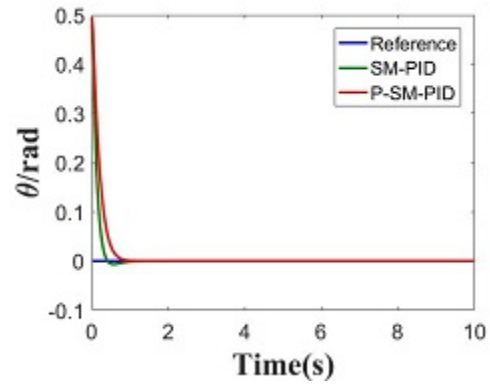
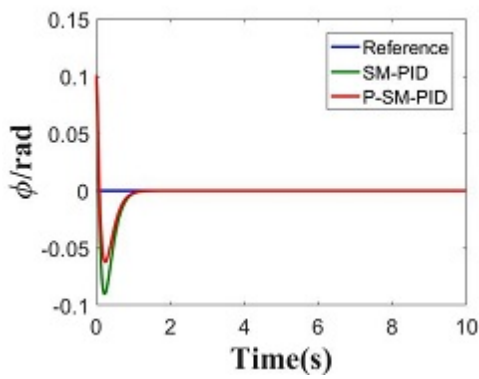
Table 2: Structure and control parameters values of controller

number	Parameters	Values
1	m_l	0.875 kg
2	g	9.8 m/s ²

3	R	0.125 m
4	I_x	0.4733 kg·m ²
5	I_z	0.2244 kg·m ²
6	C_T	1.08E-05
7	d_1	300
8	c_1	150
9	j_1	7.5
10	d_2	30
11	c_2	50
12	j_2	2
13	d_3	30
14	m_2	0.106 kg
15	L	0.225 m
16	ρ	11.69 kg/m ³
17	I_y	0.1353 kg·m ²
18	C_Q	1.90E-07
19	c_3	50
20	j_3	15

21	d_4	30
22	c_4	30
23	k_p	10
24	k_i	1
25	k_d	2

The control process of the quadrotor is as follows: first, keep x and y direction without displacement at all times, and the height of z axis rises from 0 m to 0.5 m and remains unchanged. After the target is reached, the manipulator is manipulated, and the rear manipulator is gradually changed from the original deviation angle of 0 to 30 degrees, and the angle is kept unchanged. When it is stable, it can start grasping action. For further comparison and analysis, the experimental comparison is made between the sliding mode PID and compression factor particle swarm parameter optimization sliding mode PID of piecewise cost function with the desired inclination angle of the manipulator as the edge angle of the sinusoidal motion.



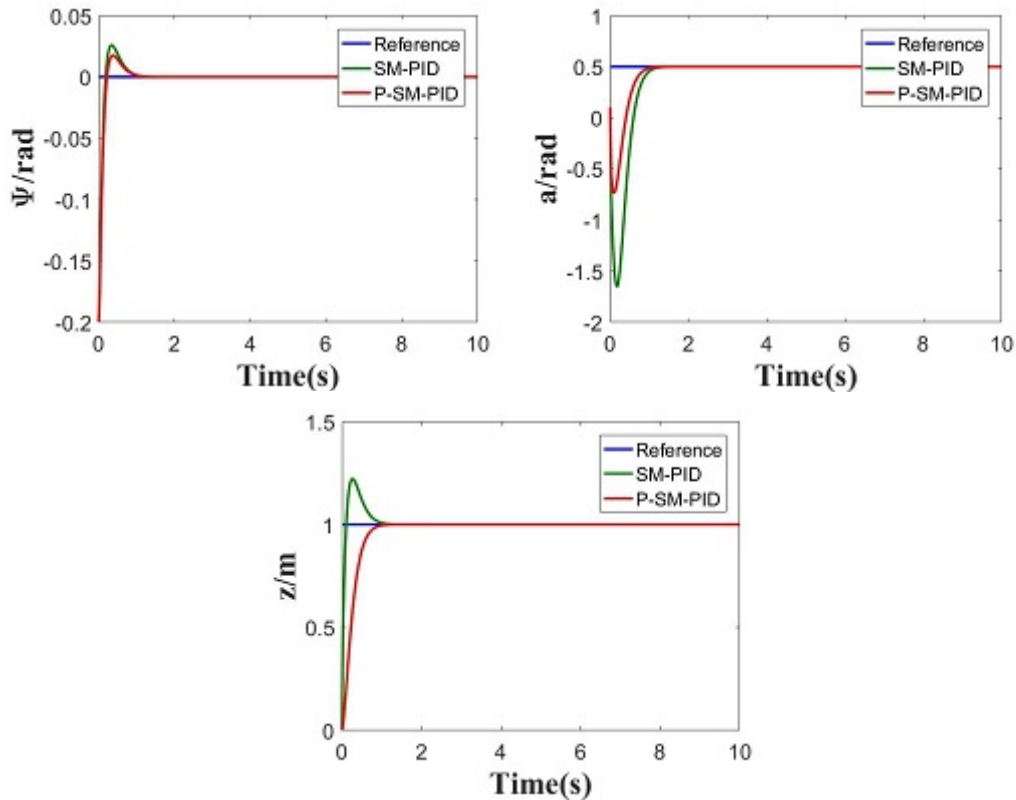


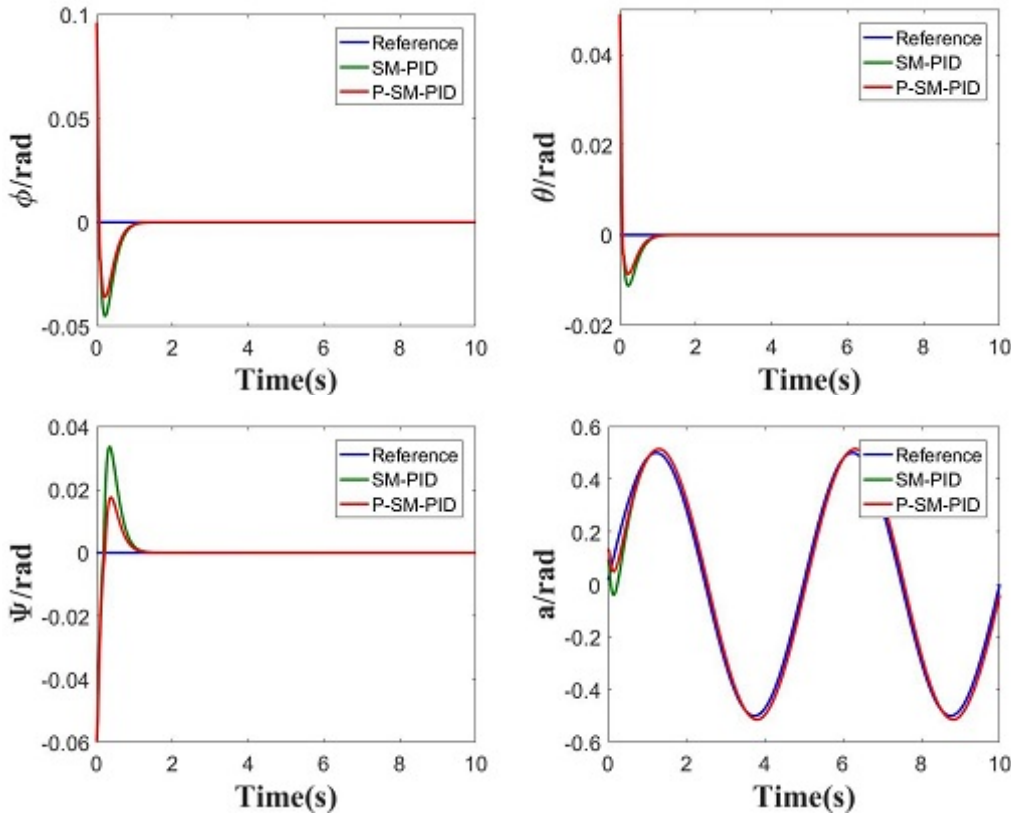
Figure 5: Attitude curve of the system under SM-PID control and PID control

Simulate through Simulink to get information on various positions and attitude angles of the quadrotors. In this paper, the stability of the quadrotor is studied and analyzed, so the attitude angle and the height of it are mainly analyzed in detail. Fig. 5 is a simulation curve obtained by optimizing sliding mode PID (P-SM-PID) control and sliding mode PID (SM-PID) control based on a piecewise cost function of the above input value and expected value. In order to compare and analyze, the PID control is designed for effect comparison.

The simulation shows that the overshoot amount of the roll angle is about -0.06 rad, the pitch angle has no overshoot, the overshoot of the yaw angle is 0.03 rad, the tilt angle and the height value of the drop-down manipulator have no overshoot in in the sliding mode PID control of compression-factor particle swarm parameters for piecewise cost function. In the SM-PID control, the overshoot is -0.09 rad, -0.02 rad, 0.03 rad, -1.7 rad and 1.23 rad respectively. The overshoot of SM-PID control is far greater than that of P-SM-PID control, the fluctuation amplitude and the flatness are larger, while P-SM-PID is more stable. The adjustment time of pitch angle and yaw angle is about 1.2 s, and that of roll angle is about 0.8 s. The height value converges to the expected value at 1.1 s. The tilt angle of the pull-down manipulator converges to the expected value at 1.2 s and remains unchanged. In contrast, the adjustment time of SM-PID in all directions will increase a lot. It is known that the expected expiration value can be converged in a shorter adjustment

time, and the rapidity is better.

Fig. 6 is a periodic sine wave with a desired angular rate of 0.2 rad/s and an amplitude of 0.5. That is, when the desired motion mode of the manipulator is in a sine state, the tracking effects of the two types of control are compared. The results show that when the expected tilt angle of the manipulator fluctuates sinusoidally, the overshoot of the flip angle and pitch angle of the P-SM-PID control is significantly reduced, and the height value has no overshoot. Moreover, the overshoot of the yaw angle in the P-SM-PID control is smaller and the adjustment time is shorter. It is known that the P-SM-PID control system is stable and fast. The overshoot of the yaw angle in the sliding mode PID control has a large fluctuation and a longer adjustment time. This is mainly due to the oscillation of the pull-down object that will affect the stability of the whole system, while the anti-interference capability of the SM-PID is not as strong as that of sliding-mode PID (P-SM-PID) control of compression factor PSO algorithm of piecewise cost function, which leads to a certain fluctuation in the overshoot of the system.



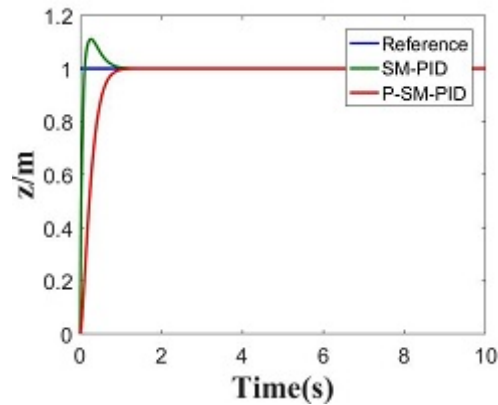


Figure 6: Figures of controlling systems' attitude curve under sinusoidal transport

7 Conclusions

In this paper, a dynamic model of a rotorcraft manipulator is established. Based on the sliding mode PID method, the controller module U, the quadrotor dynamic module Muav and the fitness module are designed based on the piecewise cost function based PSO optimization sliding mode PID (P-SM-PID) method, and the stability control of the rotorcraft manipulator is studied by establishing Lyapunov function. By comparing the simulation results of sliding mode PID (SM-PID) and piecewise cost function based PSO optimization sliding mode PID (P-SM-PID) in different environments, it is verified that the above-mentioned P-SM-PID control can reach the steady state quickly and smoothly, has good anti-interference, solves the problem of susceptible to interference in the SM-PID control process, and overcomes the serious chattering in the sliding mode control. Moreover, P-SM-PID control does not depend on external disturbance and parameter perturbation, and has strong robustness and adaptability.

Acknowledgement: This research is supported by the National Natural Science Foundation of China (51875293, 51575283, 61605083, 51605232), Key points for marine environmental security (2018YFC1405700).

Conflicts of Interest: The authors declare that they have no conflicts of interest to report regarding the present study.

References

- Chen, F. Y.; Jiang, R. Q.; Zhang, K. K.; Jiang, B.; Tao, G.** (2016): A Robust backstepping sliding-Mode control and observer-based fault estimation for a quadrotor UAV. *IEEE Transactions on Industrial Electronics*, vol. 63, no. 8, pp. 5044-5056.
- Duc, M. N.; Trong, T. N.; Xuan, Y. S.** (2015): The quadrotor MAV system using PID control. *IEEE International Conference on Mechatronics and Automation*, pp. 506-510.
- Faruk, M. S.; Kikuchi, K.** (2011): Adaptive frequency-domain equalization in digital coherent optical receivers. *Journal of Vibration & Control*, vol. 6, no. 2, pp. 573-580.

- Karagulle, H.; Malgaca, L.; Dirilmis, M.; Akdag, M.; Yavuz, S.** (2015): Vibration control of a two-link flexible manipulator. *Optics Express*, vol. 23, no. 12.
- Liu, Y. P.; Li, X. Y.; Wang, T. M.; Zhang, Y. H.; Mei, P.** (2016): Quantitative stability of quadrotor unmanned aerial vehicles. *Nonlinear Dynamics*, vol. 87, no. 3, pp. 1819-1833.
- Merheb, A. R.; Noura, H.; Bateman, F.** (2014): Active fault tolerant control of quadrotor UAV using Sliding Mode Control. *IEEE International Conference on Unmanned Aircraft Systems*, pp. 156-166.
- Mebarki, R.; Lippiello, V.** (2014): Image based control for aerial manipulation. *Asian Journal of Control*, vol. 16, no. 3, pp. 646-656.
- Purwar, S.; Kar, I. N.; Jha, A. N.** (2004): Adaptive control of robot manipulators using fuzzy logic systems under actuator constraints. *Fuzzy Sets and Systems*, vol. 152, no. 3, pp. 651-664.
- Ran, M. P.; Wang, Q.; Hou, D.; Dong, C.** (2014): Backstepping design of missile guidance and control based on adaptive fuzzy sliding mode control. *Chinese Journal of Aeronautics*, vol. 27, no. 3, pp. 634-642.
- Sathya, P. D.; Kayalvizhi, R.** (2014): Optimal multilevel thresholding using bacterial foraging algorithm. *Expert Systems with Applications*, vol. 38, no. 12, pp. 15549-15564.
- Tran, M. D.; Kang, H. J.** (2016): Adaptive terminal sliding mode control of uncertain robotic manipulators based on local approximation of a dynamic system. *Neurocomputing*, vol. 228, no. 8, pp. 231-240.
- Wang, J.; Ju, C. W.; Gao, Y.; Sangaiah, A. K.; Kim, G. J.** (2018): A PSO based energy efficient coverage control algorithm for wireless sensor networks. *Computers, Materials & Continua*, vol. 56, no. 3, pp. 433-446.
- Xiang, X. B.; Liu, C.; Su, H. S.; Zhang, Q.** (2017): On decentralized adaptive full-order sliding mode control of multiple UAVs. *ISA Transactions*, vol. 71, no. 2, pp. 196-205.
- Xie, Y.; Zhao, T.; Cai, G. P.** (2013): Dynamic modeling and active control of flexible plate based on the input-output data. *Acta Mechanica Sinica*, vol. 26, no. 3, pp. 255-262.
- Zheng, E. H.; Xiong, J. J.; Luo, J. L.** (2014): Second order sliding mode control for a quadrotor UAV. *ISA Transactions*, vol. 53, no. 4, pp. 1350-1356.